Materials Science in Additive Manufacturing

ORIGINAL RESEARCH ARTICLE

Experimental and numerical studies on the acoustic performance of simple cubic structure lattices fabricated by digital light processing

Zhejie Lai, Miao Zhao, Chong Heng Lim, Jun Wei Chua*

Department of Mechanical Engineering, National University of Singapore, 117575, Singapore

Abstract

Sound absorption is one of the important properties of porous materials such as foams and lattices. Many mathematical models in the literature are capable of modeling the acoustic properties of lattices. However, appropriate models need to be chosen for specific lattice structures on a case-by-case basis and require significant experience in acoustic modeling. This work aims to provide simplified insights into different mathematical models for the simple cubic lattice. The strut lengths and radii of the unit cells were varied, and the sound absorption properties were measured using an impedance tube. The sound absorption coefficients of the lattices generally increased and exhibited more resonant-like behavior as the strut radius increased. The Delany-Bazley (DB) model and the multi-layered micropore-cavity (MMC) model were used to simulate the acoustic properties of the lattices. The correction factors in the MMC were calculated based on empirical relations fitted using experimental data of the design geometry parameters. Results show that the DB model was able to model the sound absorption coefficients for lattice samples with porosities as low as 0.7, while the MMC with resonator theory is a more appropriate acoustics approach for lattices with porosities lower than 0.7. This work will be highly useful for materials researchers who are studying the acoustic properties of novel porous materials, as well as manufacturers of acoustic materials interested in the additive manufacturing of lattice structures for sound absorption and insulation applications.

Keywords: Lattice structures; Sound absorption; Delany-Bazley model; Transfer matrix method; Resonance

***Corresponding author:**
Jun Wei Chua
(chua.junwei@u.nus.edu)

Citation: Lai Z, Zhao M, Lim CH, *et al*., 2022, Experimental and numerical studies on the acoustic performance of simple cubic structure lattices fabricated by digital light processing. *Mater Sci Add Manuf,* 1(4): 22.
https://doi.org/10.18063/msam.v1i4.22

Received: October 6, 2022

Accepted: October 28, 2022

Published Online: November 17, 2022

1. Introduction

Porous materials have become a desired type of materials in several fields, such as sound absorption and insulation[1-5], heat exchange, chemical processing, bioengineering, and energy storage[3], due to their specific properties, including lightweight, high specific surface area, low bulk density, and microstructure controllability[6,7]. The lattice is one of the three types of porous structural categories, which is an ordered and location-specific structure that repeats the unit cell in a certain manner. In addition, the research of the theories and optimization of lattice are developed due to the additive manufacturing (AM) processing that emerged, which makes lattice fabrication possible.

One of the critical properties is acoustic performance, including sound absorption and sound insulation, which is highly structural-dependent for lattice material. In the history of AM development, various technologies emerged to overcome the difficulties of the AM processes. They can be divided into three large groups, mainly liquid-based, powder-based, and solid-based processes. In general, the liquid-based processes use photosensitive polymers as raw materials and ultraviolet (UV) light as energy source. These liquid-based technologies generally have some advantages, such as cost-effectiveness, high dimension accuracy, good surface finish, and a wide range of available materials. But they also have some shortcomings, such as post-processing requirements, relatively small build volumes, and no multi-materials capability. For solid-based processes such as material extrusion, thermoplastics filaments and metal wires are primarily used as base materials, and heat energy or electron beams are used as an energy source. The advantages of these processes include multi-material parts fabrication, ease of structure removal and minimal material wastage. However, these processes tend to suffer from relatively poor dimensional accuracies and surface finishes, limited material choices and relatively high energy consumption. In addition, as for powder-based technologies, they mainly exploit the high-energy laser and electron beam as an energy source and powder form material including thermoplastics and metals, with the latter being the more common class of materials. These technologies can present fast, with no support structure, large build volume and have additional part function processing. Furthermore, due to the lack of development, the materials are limited and surface finish and accuracy are relatively poor, and the energy consumption is the highest among the total technologies, which are the main disadvantages of the powder-based processes. The detailed information for liquid-, solid-, and powder-based technologies are summarized in Supplementary Text 1 (in Supplementary File).

While the complex interior structure of engineered lattices makes it difficult to analyze their acoustic properties, there exist many mathematical models that aim to characterize the sound absorption or transmission properties of porous materials. These models include the classical Delany-Bazley (DB) model[8], the Johnson-Champoux-Allard model[1,9], the Biot theory[10,11], and the transfer matrix method (TMM)[12,13]. Furthermore, the parameters for the above models may be obtained through measurements, analytical, or empirical methods[1,14-16]. For instance, research on the sound absorption efficiency of IN625 foams has been proposed by Zhai *et al.*[17] The classical DB model using a tetrakaidekahedral unit cell was employed to predict the performance of foams, which are fabricated through template replication processing. A good agreement between the numerical and experimental results was observed. The model was also used alongside the TMM with minor modifications to model the sound absorption properties of functionally graded metal foams with a finite number of layers with great accuracy[18].

A less conventional approach in the acoustic modeling of lattice structures is to view such lattices as resonant materials similar to Helmholtz resonators[19,20] and microperforated panels (MPP)[21,22]. In a recent work on the sound absorption performances of microlattices, the sound and energy absorption of four classes of plate and truss microlattices based on the faced-centered cubic (FCC) crystal structure were investigated[23]. Sound absorption measurements on metal lattice samples of various geometries and the number of layers revealed that there exist various numbers of resonance peaks with absorption coefficients near one. The number of resonance peaks in the frequency range corresponds to the number of layers, with the first peak occurring at the lower frequencies when the number of layers is increased. It was proposed in the work that the modeling of the characteristic impedance based on a modification of major research work by Maa *et al.*[21], which assumes the cavities as a set of micro-perforations, was a viable method that can model such lattices with great accuracies.

From the above case studies, the mechanisms of sound propagation and dissipation can be modeled by methods that may vary significantly in physics. It takes a trained researcher in the acoustics community to determine with confidence the most appropriate mathematical model to model the acoustic properties of lattice structures of a particular geometry, especially if the geometry is novel. Even for the same lattice design, the physics of sound propagation can vary widely with changes in its design parameters such as unit cell size and strut width. Such difficulty in determining the most appropriate modeling approach arises as there is very few concrete acoustics design guidelines dedicated to lattice structures in the literature.

In this work, the acoustic properties of truss lattice structures based on the simple cubic (SC) crystal structure were investigated. Many samples of SC-Truss lattices of varying unit cell lengths and strut radii were fabricated using vat photopolymerization and their sound absorption properties were measured using an impedance tube. This work also investigated the use of both the DB model and the TMM with resonator theory, referred to herein as the multi-layered micropore-cavity (MMC) model, to model the sound absorption performances of the SC-Truss lattices and compared them with the experimental results. Thereafter, some numerical models and guidelines were proposed to

accurately characterize the acoustic properties of the lattices by first choosing the correct model by a design criterion, and then calculating the most appropriate geometrical parameters or correction factors for the model based on the lattice geometry. This work will be of significant utility to materials researchers who are studying the acoustic properties of novel porous materials, as well as manufacturers of acoustic materials interested in the AM of lattice structures for sound absorption and insulation applications.

2. Experimental and numerical methods

2.1. Fabrication of simple cubic lattices

The unit cell design of the SC-Truss lattices in this work is shown in Figure 1. The unit cell is in the form of a cube with a side length D, and the struts of the unit cell is made of cylindrical rods of radius R. The unit cell was then repeated to form a lattice structure of diameter 30 mm and height 30 mm, with truncations done to model the structure as a cylindrical structure. The cylindrical shape of the lattice structures was chosen for sound absorption measurements using an impedance tube of cylindrical cross-section, as detailed in section 2.2. The ranges of strut lengths used in this work were $D \in \{3.0, 5.0, 6.0, 7,5\}$, which gave a total of 10, 6, 5, and 4 layers of unit cells in the structure, respectively. The base case in this work is one that had unit cell dimensions of D = 5.0 mm and r = 1.03 mm, which gave a relative density of 0.3 for the lattice structure. This choice of dimensions allows for comparisons with other related lattice sound absorption works done by our research team in the past[23]. The strut radii r were varied in steps of 0.2 mm such that the porosities of the lattice structures fall between 0.4 and 0.9. The list of strut lengths and radii for the lattice structures in this work is tabulated in Table 1.

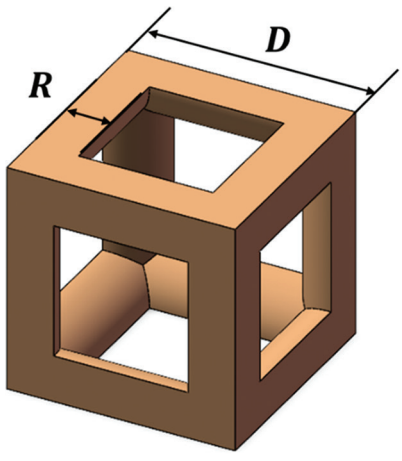

Figure 1. Schematic diagram for SC RUC with dimensions strut length D and strut radius R.

The cylindrical lattice samples were manufactured using vat photopolymerization using the Voxelab Proxima 6.0 printer. The choice of the process was derived from the comparison of the various AM processes as discussed in section 1. The solid-based and powder-based technologies, such as material extrusion and powder bed fusion, are not suited for our fabrication due to the poor surface quality of the printed samples. Moreover, compared among the market-available technologies and machines, vat photopolymerization is the most suitable AM process to be used in this work due to its reasonable material costs, a small quantity of resin during the build as well as minimal shrinkage. The resin used was the standard 405 nm UV resin from NOVA3D, chosen due to its high toughness and strength. A layer thickness of 0.05 mm and an exposure time of 2 s were used during printing. These printing parameters were determined based on the experimental determination of the optimal parameters for the printing of samples using the chosen printer and resin. As-printed parts were cleaned by immersing in isopropyl alcohol and post-cured in a UV curing chamber.

2.2. Acoustic performance characterization

The sound absorption coefficient (α) and sound transition loss were tested by the BSWA SW477 impedance tube

Table 1. Design parameters of samples

Sample	Strut length D (mm)	Strut radius R (mm)
1	3.0	0.43
2	3.0	0.63
3	3.0	0.83
4	5.0	0.63
5	5.0	0.83
6	5.0	1.03
7	5.0	1.23
8	5.0	1.43
9	6.0	0.83
10	6.0	1.03
11	6.0	1.23
12	6.0	1.43
13	6.0	1.63
14	6.0	1.83
15	7.5	1.03
16	7.5	1.23
17	7.5	1.43
18	7.5	1.63
19	7.5	1.83
20	7.5	2.03
21	7.5	2.23

based on the ISO-10534-2 standard. The average room temperature and relative humidities are 26°C and 60%, respectively. Every cylindrical SC lattice was inserted into the 30 mm diameter holder of the impedance tube. About five measurements of the sound absorption coefficients were recorded and averaged. The frequency range of interest is between 1000 Hz and 6300 Hz.

2.3. Numerical modeling of acoustic properties

In this work, the acoustic properties of the SC-Truss lattice cells were analyzed analytically using two different modeling approaches: the DB model[8,12] for porous materials and the TMM[24,25] of which some sub-domains of the air within the cells were modeled as resonant materials.

2.3.1. Delany-Bazley (DB) model

To use the DB model to simulate the sound absorption properties of the SC-Truss lattices, knowledge of their flow resistivity σ is required. These values were calculated by considering the SC-Truss unit cell as a representative unit cell (RUC) as shown in Figure 2.

According to Fourie and Du Plessis's work[26], the RUC dimension d can be calculated as a function of air volume V_a, pore size d_p, and tortuosity χ of the unit cell, given by:

$$d_{RUC} = \frac{V_a}{\chi d_p^2}. \tag{I}$$

The tortuosity χ is a geometry-dependent parameter of porous materials that characterizes the dispersion of microscopic velocity of a flowing fluid within the materials[12,26]. It can be derived in terms of the porosity φ as following:

$$\chi = 2 + 2\cos\left[\frac{4\pi}{3} + \frac{1}{3}\cos^{-1}\left(2\phi - 1\right)\right]. \tag{II}$$

Moreover, the pore dimension d_p, which is derived from the simple cubic structure, is the function of the strut length D and strut radius R as follows:

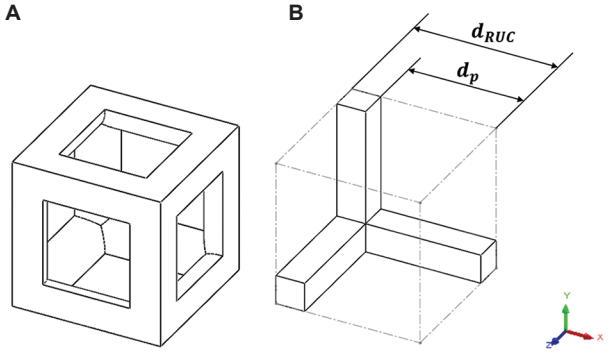

Figure 2. (A) Simple cubic unit cell. (B) Representative unit cell.

$$d_p = \frac{D}{2} - R. \tag{III}$$

The airflow resistivity σ of the SC-Truss lattices was obtained as follows[17]:

$$\sigma = \frac{36\eta\chi\left(\chi - 1\right)}{\phi^2 d_{RUC}^2}, \tag{IV}$$

Where η is the dynamic viscosity of the air at 26°C, taken as $\eta = 1.84\times10^{-5}$ kg/(m.s). Based on Equations I to IV, the airflow resistivity σ of the SC-Truss lattices was determined based on the air volume V_f, strut lengths and radii, porosity φ and the dynamic viscosity of the air within the lattice cells. Calculated values of the tortuosity χ, representative unit cell dimension d_{RUC} and airflow resistivity σ are tabulated in Supplementary Text 2 in the Supplementary File.

2.3.2. Multi-layered micropore-cavity (MMC) model

The MMC model is a mathematical model that integrates the use of the TMM and the theories of MPPs to model the sound propagation in multi-layered Helmholtz Resonator structures. Unlike the DB model that views the SC-Truss lattices as homogeneous porous materials, this model views the lattices as multiple layers of micropores with air cavities in between. The TMM is a powerful analytical method to model the propagation of acoustic waves in one-dimensional problems involving multiple discrete layers of acoustic material[12,27]. The general expression of the TMM for n heterogeneous layers in series is as follows:

$$\begin{Bmatrix} p \\ v_y \end{Bmatrix}_{x=0} = \left[\boldsymbol{T}_{layer\,1}\right]\left[\boldsymbol{T}_{layer\,2}\right]\cdots\left[\boldsymbol{T}_{layer\,n}\right]\begin{Bmatrix} p \\ v_y \end{Bmatrix}_{x=L} = \left[\boldsymbol{T}_{total}\right]\begin{Bmatrix} p \\ v_y \end{Bmatrix}_{x=t} = \begin{bmatrix} T_{11} & T_{12} \\ T_{21} & T_{22} \end{bmatrix}\begin{Bmatrix} p \\ v_y \end{Bmatrix}_{x=L}, \tag{V}$$

where $\left[\boldsymbol{T}_{layer\,x}\right]$ is the transfer matrix for Layer x. To model the acoustic properties of the SC-Truss lattices using the TMM, the air domain within the SC-Truss unit cell, as shown in Figure 1, needs to be discretized into sub-domains and the acoustic properties determined individually. The sub-domains consist of two narrow tubes of square cross-section and a central open cavity similar to that of the unit cell, as shown in Figure 3. The narrow tubes on both ends of the cavity have a side length of d_{tube} = D – 2R and a thickness of $t_{tube} = \frac{R}{\sqrt{2}}$. The latter dimension results from the cylindrical cross-sectional geometry of the individual struts. The cavity is then modeled as a layer of air of thickness $l_{cav} = D - 2t_{tube} = D - \sqrt{2}R$.

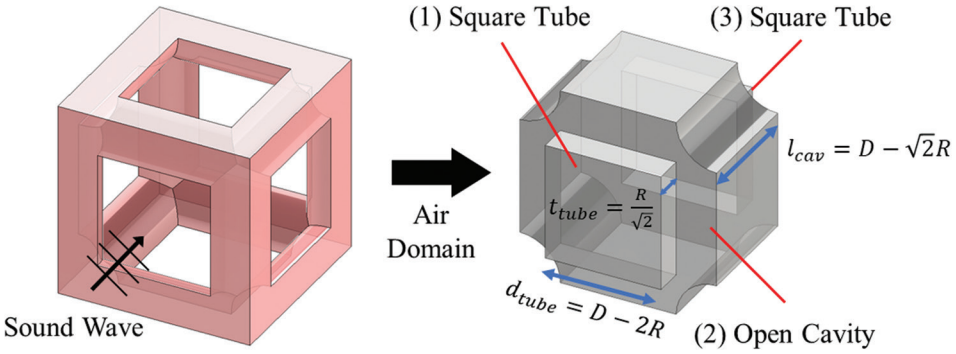

Figure 3. Discretization of the air domain of the SC-Truss unit cell for the acoustic modeling using the MMC model.

By assuming the closed tubes of square cross-section as a set of resonant materials, the transfer matrix is given by[25]

$$\boldsymbol{T}_r = \begin{bmatrix} 1 & Z_r \\ 0 & 1 \end{bmatrix}, \tag{VI}$$

Where Z_r is the characteristic impedance of the closed tube. Based on the works by Maa, Morse and Ingard[21,22] on microperforated panel absorbers, Z_r can be expressed as follows:

$$Z_r = \frac{32\eta t_{tube}}{\varepsilon d_{tube}^2}\left(\sqrt{1+\frac{k^2}{32}} + 2\delta_1 R_s\right) + j\frac{\omega\rho_0 t_{tube}}{\varepsilon}\left(1+\frac{1}{\sqrt{9+\frac{k^2}{2}}}+\delta_2\frac{d_{tube}}{t_{tube}}\right), \tag{VII}$$

Where η, ρ_0 refer to the dynamic viscosity and density of air at 25°C respectively, ω is the angular frequency of the sound waves, j is the imaginary unit such that $j^2 = -1$, ε is the perforation ratio of the square tubes given by $\varepsilon = \left(\frac{d_{tube}}{D}\right)^2$, $k = \left(\frac{d_{tube}}{2}\right)\sqrt{\frac{\rho\omega}{\eta}}$ is the perforate constant, and $R_s = \frac{1}{2}\sqrt{2\eta\rho_0\omega}$ is the resistive end-correction factor that accounts for the air friction arising from the oscillatory viscous flow on the surface of the perforated panel. δ_1 and δ_2 are the resistive and reactive correction factors to be determined from experimentally determined sound absorption coefficient results from this work.

For the open cavity of the SC-Truss unit cell, the layer was simply modeled as a layer of air of density ρ_0 and speed of sound c_0, similar to the air outside the lattice cells. The transfer matrix of the cavity is given by[25].

$$\boldsymbol{T}_c = \begin{bmatrix} \cos(k_0 l_{cav}) & jZ_0\sin(k_0 l_{cav}) \\ j\frac{1}{Z_0}\sin(k_0 l_{cav}) & \cos(k_0 l_{cav}) \end{bmatrix}, \tag{VIII}$$

Where $Z_0 = \rho_0 c_0$ and $k_0 = \frac{\omega}{c_0}$ are the characteristic impedance and the wave number of the air layer, respectively. Thereafter, the transfer matrix of one layer of SC-Truss unit cells is given by,

$$\left[\boldsymbol{T}_{layer\,x}\right] = \boldsymbol{T}_r\boldsymbol{T}_c\boldsymbol{T}_r = \begin{bmatrix} 1 & Z_r \\ 0 & 1 \end{bmatrix} \begin{bmatrix} \cos(k_0 l_{cav}) & jZ_0\sin(k_0 l_{cav}) \\ j\frac{1}{Z_0}\sin(k_0 l_{cav}) & \cos(k_0 l_{cav}) \end{bmatrix} \begin{bmatrix} 1 & Z_r \\ 0 & 1 \end{bmatrix}. \tag{IX}$$

The sound absorption coefficient is a measure of the proportion of sound energy absorbed and dissipated by a material when a sound wave is incident on it and is commonly used to quantify the sound absorption capability of a material[28]. An estimate of the sound absorption coefficient α_{TMM} for each frequency f for the multi-layered material can be determined directly for T_{total} by the following expression[25]:

$$\alpha_{TMM}(f) = 1 - \left|\frac{T_{11} - \frac{\rho_0 c_0 T_{21}}{\cos\theta}}{T_{11} + \frac{\rho_0 c_0 T_{21}}{\cos\theta}}\right|^2, \tag{X}$$

Where θ is the angle of incidence of the sound wave. For normal incidence, $\theta = 0°$ and hence $\cos\theta = 1$.

Based on experimental data, the optimal values of the correction factors δ_1 and δ_2 were determined and their relations to the geometric parameters of the SC-Truss unit cell were proposed. Thereafter, α_{TMM} for each case were

calculated with δ_1 and δ_2 calculated from the proposed models. The mean absolute error of the absorption coefficients over the entire frequency range was obtained for each case. The calculated values of tube side length d_{tube}, tube thickness t_{tube}, cavity layer thickness l_{cav}, and the perforation ratio ε are tabulated in Supplementary Text 2 in the Supplementary File.

3. Results

3.1. Manufacturing of samples and dimensional analysis

Representative macroscopic and microscopic sample images are presented in Figure 4A and 4B, respectively. The rest of the macroscopic and microscopic sample images are presented in Supplementary Texts 3 and 4, respectively. The strut lengths and radii of the samples were measured under the digital microscope using pixel measurement. At least three measurements of both the strut lengths and radii were taken, and the arithmetic averages were obtained. The percentage error in dimensions was calculated using Equation XI below.

$$Percentage\,error = \frac{\left|\text{Measured dimension} - \text{Design dimension}\right|}{\text{Design dimension}} \times 100\% \quad \text{(XI)}$$

The design dimensions, actual dimensions, and dimension error percentages are tabulated in Table 2. It is obvious that all the actual dimension values were close to the designed values the error percentages were approximately 0%–2% and several cases were about 3%–4%. In general, the percentage dimension errors were acceptable and hence the design dimensions may be used in subsequent analytical analysis without a need for error corrections.

3.2. Sound absorption coefficients of SC-Truss lattice structures

The sound absorption coefficients of all the SC-Truss lattices are plotted in Figure 5. Each of the plots of sound frequencies with sound absorption coefficients was of the same strut length. The mean and standard deviations of the absorption coefficients are also plotted in Figure 5.

Overall, for fixed strut lengths, the average sound absorption performance of the SC-Truss lattice was enhanced when the strut radius was increased. The mean absorption coefficients generally increased with increasing strut radius. The variations in sound absorption coefficients became more fluctuating with increasing strut radius with fixed strut length. This can also be observed from the higher standard deviations of the absorption coefficients with increasing strut radii. In addition, when the curves showed the peak and valley characteristics, increasing the strut radius resulted in the reduced frequency of the first peak absorption coefficient and a higher coefficient value at the first peak frequency.

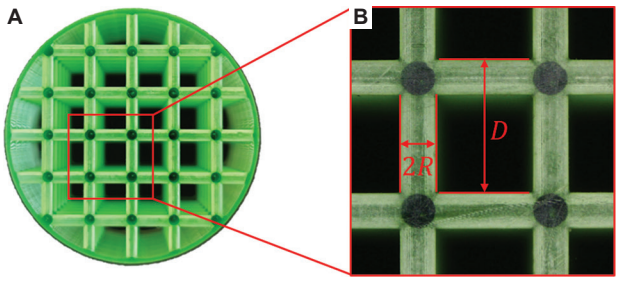

Figure 4. (A) Macroscopic sample image. (B) Microscopic sample image. Abbreviations: *D*, strut length; *R*, strut radius.

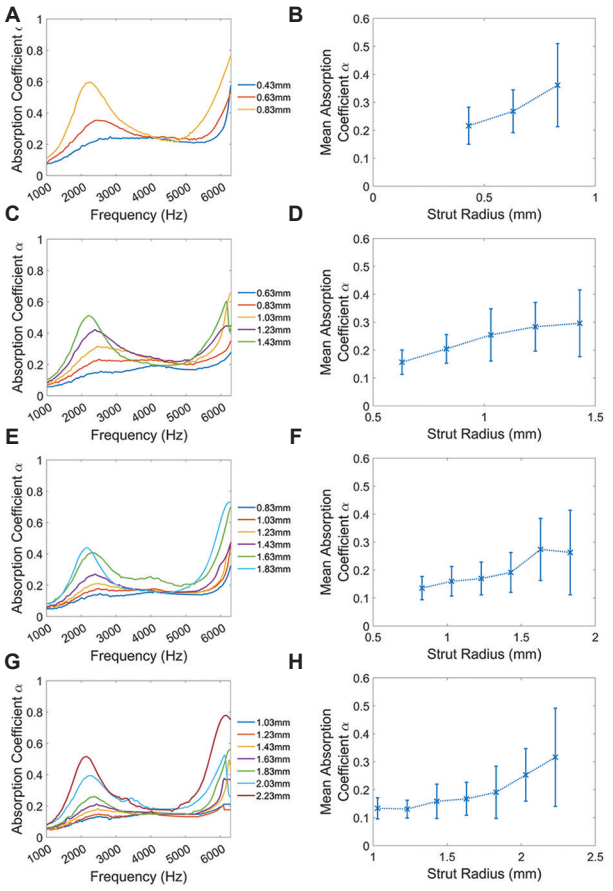

Figure 5. Plots of the sound absorption coefficients obtained from experimental measurements. (A) and (B) correspond to the cases for D = 3 mm, (C) and (D) correspond to the cases for D = 5 mm, (E) and (F) correspond to the cases for D = 6 mm, and (G) and (H) correspond to the cases for D = 7.5 mm. (A), (C), (E), and (G) correspond to the cases where d is the smallest among cases with the same D, while (B), (D), (F), and (H) correspond to the cases where d is the largest amongst cases with the same D.

Table 2. Dimension analysis of the fabricated lattice samples

Sample	Strut length *D* (mm)			Strut radius *R* (mm)		
	Design	Measured	Percentage error	Design	Measured	Percentage error
1	3.0	2.99	0.22	0.43	0.44	1.55
2	3.0	3.00	0.11	0.63	0.65	3.44
3	3.0	2.98	0.78	0.83	0.83	0.20
4	5.0	4.99	0.27	0.63	0.66	4.76
5	5.0	5.00	0.00	0.83	0.81	2.41
6	5.0	5.01	0.13	1.03	1.02	1.29
7	5.0	5.00	0.00	1.23	1.22	1.08
8	5.0	4.97	0.53	1.43	1.44	0.70
9	6.0	6.02	0.39	0.83	0.86	3.01
10	6.0	6.03	0.44	1.03	1.04	0.65
11	6.0	6.01	0.22	1.23	1.25	1.76
12	6.0	6.04	0.61	1.43	1.45	1.17
13	6.0	6.02	0.28	1.63	1.65	1.12
14	6.0	6.03	0.50	1.83	1.84	0.27
15	7.5	7.53	0.40	1.03	1.05	2.10
16	7.5	7.53	0.40	1.23	1.25	1.76
17	7.5	7.53	0.44	1.43	1.46	1.75
18	7.5	7.53	0.40	1.63	1.64	0.51
19	7.5	7.51	0.18	1.83	1.86	1.73
20	7.5	7.53	0.36	2.03	2.07	1.72
21	7.5	7.51	0.13	2.23	2.25	0.67

3.3. Numerical modeling of sound absorption performances

3.3.1. Delany-Bazley (DB) model

Representative plots of the sound absorption coefficients obtained from the DB model are shown in Figure 6. For each strut length, the strut radii used for the plots are the smallest and largest among the cases of the same strut length. The comparison plots for all the test cases in this work are collated in Supplementary Text 5 in the Supplementary File. It can be seen that for small strut radii, the DB model generally modeled the general increase in absorption coefficients with increasing frequencies reasonably well. That being said, the model tends to underestimate the sound absorption coefficients, especially at high frequencies. These under-estimation issues were more apparent for higher strut lengths. For large strut radii, the DB model was able to model the peak absorption behaviors at low frequencies. However, the peak absorption coefficients predicted by the DB model tend to be slightly larger than the experimental values. Furthermore, the DB model was not able to correctly model the high sound absorption peaks at higher frequencies above 5000 Hz, instead the model predicted significantly lower sound absorption coefficients at those frequencies. It is noted that the DB model was derived to model the sound absorption performances of porous materials of high porosity such as synthetic foams. Therefore, it was likely that the DB model was not able to accurately model the sound absorption performances of porous materials of moderate porosity, such as the lattices in this work with high strut radii.

3.3.2. Multi-layered micropore-cavity (MMC) model

Using different pairs of values for the correction factors δ_1 and δ_1, the sound absorption coefficients over the frequency range of interest were calculated using the MMC model as described in section 2.3.2. Thereafter, the optimal $\{\delta_1, \delta_2\}$ pair was chosen based on the mean absolute errors in sound absorption coefficients as compared with the experimental values. The optimal values of δ_1 and δ_2 for each test case were collated in Supplementary Text 6 in the Supplementary File. It was proposed that the correction factors δ_1 and δ_2 may be dependent on the geometry of the narrow tubes or the lattice samples, such as the tube side length d_{tube}, tube thickness t_{tube}, perforation ratio ε, and the

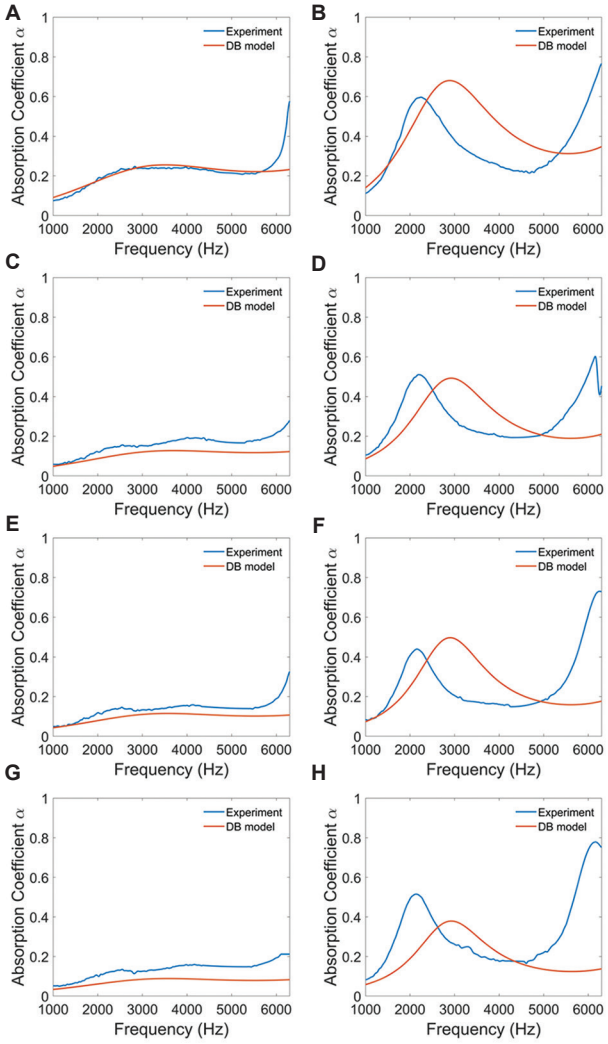

Figure 6. Plots of the sound absorption coefficients obtained from both experimental measurements and numerical modeling using the DB model. (A) and (B) correspond to the cases for D = 3 mm, (C) and (D) correspond to the cases for D = 5 mm, (E) and (F) correspond to the cases for D = 6 mm, and (G) and (H) correspond to the cases for D = 7.5 mm. (A), (C), (E), and (G) correspond to the cases where d is the smallest amongst cases with the same D, while (B), (D), (F), and (H) correspond to the cases where d is the largest amongst cases with the same D.

number of unit cell layers N in the lattice samples. Observations of the data revealed that δ_1 could be a function of $\frac{d_{tube}}{t_{tube}}$ and N, as shown in the plot of $\frac{d_{tube}}{t_{tube}}$ against $N\delta_1$ in Figure 7A. Linear regression was done on the data points and the data points seem to lie close to the regression line with $R^2 = 0.8547$. The regression line has the following equation:

$$N\delta_1 = 183.0961\frac{d_{tube}}{t_{tube}} - 109.0583 \quad \text{(XII)}$$

Similarly, δ_1 could be a function of the perforation ratio ε (Figure 7B). Such a hypothesis is because the reactance correction factor is already a function of $\frac{d_{tube}}{t_{tube}}$ and similar hypothesis on δ_2 were made in the previous works[29]. However, it can be seen that δ_2 was zero when the perforation ratio was too low or too high, while δ_2 peaks when the perforation ratio is around 0.35. Henceforth, it was proposed that the data points are divided into two equal subsets based on the porosity φ of the lattice samples. By applying linear regression on each of the subsets, the following empirical piecewise relation for δ_2 was obtained:

$$\delta_2 = \begin{cases} 1.9320\varepsilon - 0.3012 \; for \phi < 0.6893 \\ -0.7545\varepsilon + 0.5879 \; for \phi < 0.6893 \end{cases} \quad \text{(XIII)}$$

The coefficients of determination R^2 for the two linear regression lines were 0.8629 and 0.4782, respectively. While the first regression line fits the data points well, the linear correlation between the perforation ratio and δ_2 was relatively weak, owing to the large variations in values of δ_2 at higher porosities.

Representative plots of the sound absorption coefficients obtained from the DB model are shown in Figure 8. Similar to Figure 6, the strut radii used for the plots are the smallest and largest strut radii among the cases of the same strut length. The comparison plots for all the test cases in this work were collated in Supplementary Text 7 in the Supplementary File. Based on the observation from the figure for small strut radii, the MMC model was also appropriate in simulating the sound absorption behavior throughout the frequency range. However, the deviations from the experimental results were slightly larger than that of the DB model due to the higher peak frequencies at frequencies below 4000 Hz predicted by the MMC model. Unlike the DB model, the MMC model was able to model the sound absorption properties of lattices of larger strut radii more closely to the experimental results. Such good fitting of experimental results can be reasoned that the cross-sectional area of the square tubes in Figure 3 was sufficiently small such that they bear closer resemblances to conventional MPPs in the literature. Moreover, the use of empirical relations in Equations XII and XIII assisted in shifting the sound absorption curves closer to the experimental data due to how the relations were derived. Hence, it can be concluded that the MMC model was a better mathematical model to model the sound absorption properties of lattices with large strut radii.

3.3.3. Mean absolute errors in absorption coefficients

The plot of the mean percentage errors of the absorption coefficients based on the DB model and the MMC model is

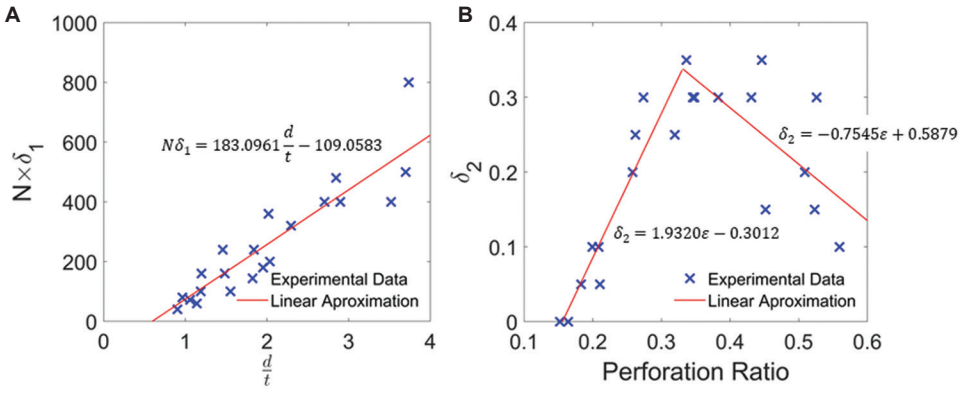

Figure 7. (A) Plot of $\frac{d_{tube}}{t_{tube}}$ against $N\delta_1$, with the plot and equation of the linear approximation of the experimental data. (B) The plot of the perforation ratio ε against δ_2, with the plots and equations of the piecewise linear approximations of the experimental data.

shown in Figure 9. Values of the mean percentage errors are provided in Supplementary Text 8 in the Supplementary File. It can be seen that the DB model resulted in percentage errors of mostly between 5% and 60%, with most of the errors being around 20%–30%. Notably, the mean percentage error is the lowest at 8.5% for the sample with D = 3.0 mm and R = 0.43 mm. The percentage errors for low porosity lattices (φ < 0.5) were noticeably high at above 40%. This is expected considering the low accuracy of the DB model for low-porosity materials. In contrast, the percentage errors from the MMC model were relatively lower than that of the DB model at around 10%–20% for most lattice samples. Moreover, the MMC model predicted the sound absorption performances significantly better than the DB model for lattice samples with porosities below 0.7, while the percentage errors were comparable to the DB model for porosities above 0.7. Hence, one can infer that for SC-Truss lattices with porosities below 0.7, the MMC model is a more accurate model to calculate the sound absorption coefficients. For SC-Truss lattices with porosities above 0.7, both the DB model and the MMC model work similarly well in predicting the sound absorption coefficients. That being said, it is recommended to use the DB model over the MMC model due to the simplicity of the DB model.

4. Discussion

First, this work demonstrated the good dimensional accuracies of the SC-Truss lattice samples fabricated using the vat photopolymerization process. As compared to other AM processes such as material extrusion, powder bed fusion, and material jetting, the major manufacturing defects such as surface roughness and micro-porosities are less apparent in the fabricated samples[5]. Therefore, this observation proved useful in the characterization of the acoustic properties of lattice structures manufactured using AM, as the design geometrical parameters may be used in the mathematical models without much concern over corrections to the geometry. Furthermore, the photopolymer resin used in this work was notable for its high toughness and strength and has been used in previous works with high build quality and high dimensional accuracies[30,31]. Hence, the sound absorption of these lattices by structural vibrations and material damping may be neglected[12,32], which simplifies the acoustic analysis significantly.

Second, it is understood that there exists a set of criteria in which the DB model is valid[12,33]. In particular, it is acknowledged that the DB model works well only when the porosity of the porous material is close to one. Through this work, it is determined that the DB model may be able to model the acoustic properties of SC-Truss lattices for porosities above 0.7, though percentage errors of about 20% are expected. Hence, to fabricate such lattices on a large scale for industrial applications, the DB model is still applicable and can be used to determine a general trend in the variation of sound absorption coefficients with frequency. The simplicity of the DB model expressions, as well as the availability of several methods of determining the airflow resistivity of the fabricated lattices[26,34], ensures that the model is a more attractive mathematical model to use as compared to other more complicated models, such as the JCA model[12].

Finally, the determination of both δ_1 and δ_2 through experimentation and statistical regression is an approach that is less reported in the modeling of acoustic materials using the theories related to the MPP absorbers. One of the first works to do so is the work by Maa, Morse and Ingard, which assigned discrete values to δ_1 and δ_2 based on the general morphology of the narrow perforations[21,22]. Common values for δ_1 are 2 and 4, depending on whether

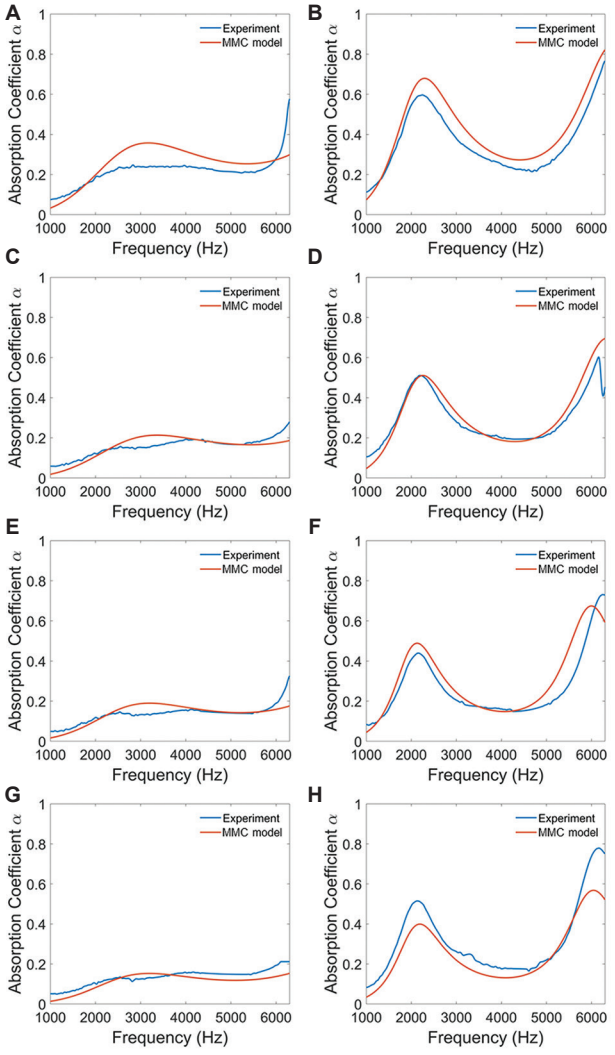

Figure 8. Plots of the sound absorption coefficients obtained from both experimental measurements and numerical modeling using the MMC model. (A) and (B) correspond to the cases for D = 3 mm, (C) and (D) correspond to the cases for D = 5 mm, (E) and (F) correspond to the cases for D = 6 mm, and (G) and (H) correspond to the cases for D = 7.5 mm. (A), (C), (E), and (G) correspond to the cases where d is the smallest amongst cases with the same D, while (B), (D), (F), and (H) correspond to the cases where d is the largest amongst cases with the same D.

the edges of the holes were round or sharp, respectively, which several prior works using Maa's formulation set δ_2 as 0.85[21,30,31,35]. However, this work has shown that such crude choices of δ_1 and δ_2 may not be effective in the context of lattice structures due to the vast difference in length scales and pore shapes. Rather, the values may be related to the detailed geometry of the lattice unit cells and pores and must be determined on a case-by-case basis. For the SC-Truss, no research works have documented the process of determining appropriate expressions for δ_1 and δ_2 for the MMC model to model the sound absorption

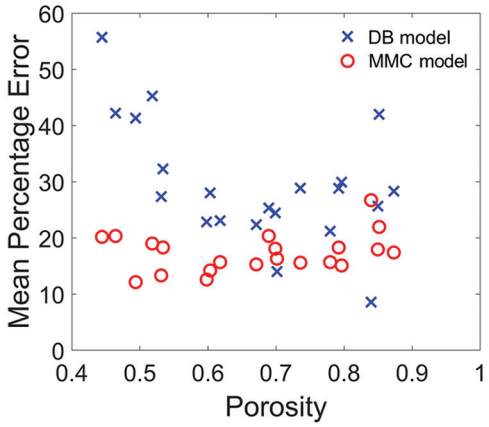

Figure 9. Plot of the porosity of the SC-Truss lattices against the mean percentage errors of the sound absorption coefficients obtained from experiments and numerical models.

properties with high accuracies. Therefore, this work is a valuable contribution to both the acoustics and materials community in determining appropriate expressions of the correction factors so that researchers and manufacturers may use the MMC model to predict the sound absorption or transmission properties of the SC-Truss lattices without having to be too concerned about the correctness of the correction factors in the model.

5. Conclusions

In this work, the acoustic properties of truss lattice structures based on the SC crystal structure were investigated. Many samples of SC-Truss lattices of varying unit cell lengths and strut radii were fabricated using vat photopolymerization, and their sound absorption properties were measured using an impedance tube. It was shown that as the strut radius increases, the sound absorption performances generally increase and become more resonant-like. This work also investigated the use of both the DB model and the MMC model to model the sound absorption performances of the SC-Truss lattices and compared them with the experimental results. It was determined that the correction factors in the MMC model may be calculated based on the empirical relation given in Equations XII and XIII, using present design geometry parameters. Furthermore, it was determined that the DB model was able to model the sound absorption coefficients for lattice samples with porosities as low as 0.7, hence seemingly stretching the limits of the validity of the model. For lattices with porosities lower than 0.7, the MMC model is a more appropriate acoustics approach than the DB model. This work will be of significant utility to materials researchers who are studying the acoustic properties of novel porous materials, as well as manufacturers of

acoustic materials interested in the AM of lattice structures for sound absorption and insulation applications.

Acknowledgments

The authors would also like to acknowledge Dr. Wei Zhai, Dr. Xinwei Li, and Dr. Xiang Yu for their supervision and valuable suggestions on the research work.

Funding

This research is supported by the NUS R&G Postdoc Fellowship Program (Project No. A-0000065-25-00).

Conflict of interest

The authors declare that they have no known competing financial interests or personal relationships that could have appeared to influence the work reported in this paper. Any opinions, findings, and conclusions or recommendations expressed in this material are those of the author(s) and do not reflect the views of National University of Singapore (NUS).

Author contributions

Conceptualization: Zhejie Lai, Jun Wei Chua
Investigation: Zhejie Lai, Miao Zhao, Chong Heng Lim
Methodology: Zhejie Lai, Miao Zhao, Chong Heng Lim, Jun Wei Chua
Resources: Chong Heng Lim
Supervision: Jun Wei Chua
Validation: Zhejie Lai, Jun Wei Chua
Writing – original draft: Zhejie Lai, Jun Wei Chua
Writing – review & editing: Jun Wei Chua

References

1. Cao L, Fu Q, Si Y, *et al*., 2018, Porous materials for sound absorption. *Composites Commun,* 10: 25–35

   https://doi.org/10.1016/j.coco.2018.05.001

2. Jia C, Li L, Liu Y, *et al*., 2020, Highly compressible and anisotropic lamellar ceramic sponges with superior thermal insulation and acoustic absorption performances. *Nat Commun*, 11: 3732.

   https://doi.org/10.1038/s41467-020-17533-6

3. Yu X, Lu Z, Zhai W, 2021, Enhancing the flow resistance and sound absorption of open-cell metallic foams by creating partially-open windows. *Acta Mater,* 206: 116666.

   https://doi.org/10.1016/j.actamat.2021.116666

4. Yang W, An J, Chua CK, *et al*., 2020, Acoustic absorptions of multifunctional polymeric cellular structures based on triply periodic minimal surfaces fabricated by stereolithography. *Virtual Phys Prototyp*, 15: 242–249.

   https://doi.org/10.1080/17452759.2020.1740747

5. Zieliński TG, Opiela KC, Pawłowski P, *et al*., 2020, Reproducibility of sound-absorbing periodic porous materials using additive manufacturing technologies: Round robin study. *Additive Manuf,* 36: 101564.

   https://doi.org/10.1016/j.addma.2020.101564

6. Cheng Y, Xu Z, Chen S, *et al*., 2021, The influence of closed pore ratio on sound absorption of plant-based polyurethane foam using control unit model. *Appl Acoust*, 180: 108083.

   https://doi.org/10.1016/j.apacoust.2021.108083

7. Doutres O, Atalla N, Dong K, 2011, Effect of the microstructure closed pore content on the acoustic behavior of polyurethane foams. *J Appl Phys,* 110: 064901.

   https://doi.org/10.1063/1.3631021

8. Delany ME, Bazley EN, 1970, Acoustical properties of fibrous absorbent materials. *Appl Acoust,* 3: 105–116.

   https://doi.org/10.1016/0003-682X(70)90031-9

9. Kino N, 2015, Further investigations of empirical improvements to the Johnson-Champoux-Allard model. *Appl Acoust,* 96: 153–170.

   https://doi.org/10.1016/j.apacoust.2015.03.024

10. Biot MA, 1956, Theory of propagation of elastic waves in a fluid-saturated porous solid. II. Higher frequency range. *J Acoust Soc Am,* 28: 179–191.

    https://doi.org/10.1121/1.1908241

11. Dib L, Bouhedja S, Amrani H, 2015, Mechanical parameters effects on acoustic absorption at polymer foam. *Adv Mater Sci Eng,* 2015: 1–10.

    https://doi.org/10.1155/2015/896035

12. Allard JF, Atalla N, 2009, Propagation of Sound in Porous media: Modelling Sound Absorbing Materials. 2nd ed. Wiley, Hoboken, N.J. p358.

13. Verdiere K, Panneton R, Elkoun S, *et al*., Transfer matrix method applied to the parallel assembly of sound absorbing materials. *J Acoust Soc Am*, 134: 4648.

    https://doi.org/10.1121/1.4824839

14. Niskanen M, Groby JP, Duclos A, *et al*., 2017, Deterministic and statistical characterization of rigid frame porous materials from impedance tube measurements. *J Acoust Soc Am,* 142: 2407.

    https://doi.org/10.1121/1.5008742

15. Boulvert J, Cavalieri T, Costa-Baptista J, *et al*., Optimally graded porous material for broadband perfect absorption of sound. *J Appl Phys*, 126: 175101.

    https://doi.org/10.1063/1.5119715

16. Chen S, Lei S, Zhu J, *et al*., 2021, The influence of microstructure on sound absorption of polyurethane foams through numerical simulation. *Macromol Theory Simul,* 30: 2000075.

https://doi.org/10.1002/mats.202000075

17. Zhai W, Yub X, Song X, *et al.*, 2018, Microstructure-based experimental and numerical investigations on the sound absorption property of open-cell metallic foams manufactured by a template replication technique. *Mater Design*, 137: 108–116.

    https://doi.org/10.1016/j.matdes.2017.10.016

18. Chua JW, Li X, Li T, *et al.*, 2022, Customisable sound absorption properties of functionally graded metallic foams. *J Mater Sci Technol*, 108: 196–207.

    https://doi.org/10.1016/j.jmst.2021.07.056

19. Gai XL, Xing T, Li XY, *et al.*, 2016, Sound absorption of microperforated panel mounted with helmholtz resonators. *Appl Acoust,* 114: 260–265.

    https://doi.org/10.1016/j.apacoust.2016.08.001

20. Komkin AI, Mironov MA, Bykov AI, 2017, Sound absorption by a Helmholtz resonator. *Acoust Phys,* 63: 385–392.

    https://doi.org/10.1134/s1063771017030071

21. Maa DY, 1998, Potential of microperforated panel absorber. *J Acoust Soc Am,* 104: 2861–2866.

    https://doi.org/10.1121/1.423870

22. Morse PM, Ingard KU, 1968, Theoretical Acoustics (International Series in Pure and Applied Physics). McGraw-Hill, New York.

23. Li X, Yu X, Chua JW, *et al.*, 2021, Microlattice metamaterials with simultaneous superior acoustic and mechanical energy absorption. *Small,* 17: e2100336.

    https://doi.org/10.1002/smll.202100336

24. Doutres O, Atalla N, Osman H, 2015, Transfer matrix modeling and experimental validation of cellular porous material with resonant inclusions. *J Acoust Soc Am,* 137: 3502–3513.

    https://doi.org/10.1121/1.4921027

25. Jiménez N, Umnova O, Groby JP, 2021, Acoustic Waves in Periodic Structures, Metamaterials, and Porous Media (Topics in Applied Physics). Springer, Germany.

26. Fourie JG, Du Plessis JP, 2002, Pressure drop modelling in cellular metallic foams. *Chem Eng Sci*, 57: 2781–2789.

    https://doi.org/10.1016/s0009-2509(02)00166-5

27. Verdière K, Panneton R, Elkoun S, *et al.*, 2013, Transfer matrix method applied to the parallel assembly of sound absorbing materials. *J Acoust Soc Am,* 134: 4648–4658.

    https://doi.org/10.1121/1.4824839

28. Ashby M, Evans T, Fleck NA, 2000, Metal Foams: A Design Guide. Elsevier, Burlington.

29. Okuzono T, Nitta T, Sakagami K, 2019, Note on microperforated panel model using equivalent-fluid-based absorption elements. *Acoust Sci Technol*, 40: 221–224.

    https://doi.org/10.1250/ast.40.221

30. Li X, Yu X, Zhai W, 2021, Additively manufactured deformation-recoverable and broadband sound-absorbing microlattice inspired by the concept of traditional perforated panels. *Adv Mater,* 33: e2104552.

    https://doi.org/10.1002/adma.202104552

31. Li X, Yu X, Zhai W, 2022, Less is more: Hollow-truss microlattice metamaterials with dual sound dissipation mechanisms and enhanced broadband sound absorption. *Small,* 18: e2204145.

    https://doi.org/10.1002/smll.202204145

32. Rahimabady M, Statharas EC, Yao K, *et al.*, Hybrid local piezoelectric and conductive functions for high performance airborne sound absorption. *Appl Phys Lett,* 111: 241601.

    https://doi.org/10.1063/1.5010743

33. Egab L, Wang X, Fard M, 2014, Acoustical characterisation of porous sound absorbing materials: A review. *Int J Veh Noise Vib* 10: 129–149.

    https://doi.org/10.1504/IJVNV.2014.059634

34. Institution BS, 1993, Acoustics. Materials for Acoustical Applications. Determination of Airflow Resistance. British Standards Institution, United Kingdom.

35. Khosravani MR, Reinicke T, 2021, Experimental characterization of 3D-printed sound absorber. *Eur J Mech A Solids*, 89: 104304.

    https://doi.org/10.1016/j.euromechsol.2021.104304